ChemPubSoc Europe

DOI: 10.1002/chem.201604775

CHEMISTRY A European Journal Full Paper

Surface Chemistry

On-Surface Dual-Response Structural Transformations of Guanine Molecules and Fe Atoms

Chi Zhang[+], Likun Wang[+], Lei Xie, Yuanqi Ding, and Wei Xu*[a]

Abstract: Structural transformation of metal–organic nanostructures holds great promise for structural diversity and flexibility and opens the way towards an adaptive and evolutive chemistry owing to the dynamic characteristic of coordination bonds. It is thus generally interesting and also challenging to develop systems showing reversible structural transformations which involve multiple metal–organic motifs on surfaces. Here, we have successfully constructed a system that presents structural transformations on a solid surface, in which controllable formation of multiple metal–organic nanostructures (with different coordination binding modes by use of distinct binding sites) in response to both metal atoms and molecules is achieved at room temperature (RT) under ultrahigh vacuum (UHV) conditions. The key to making these interconversions successful is the intrinsic dynamic characteristic of coordination bonds together with the coordination priority and diversity.

Introduction

Metal–organic coordination chemistry, which holds great promise for structural diversity, flexibility and geometrical control, has rapidly developed in the past decades.[1–3] Various metal–organic architectures have been successfully designed, regulated and organized into desired patterns and dimensions.[1–6] Structural transformation of metal–organic structures, which relies on reorganization of components by breakage and reformation of bonds to achieve change in constitution,[7–9] has opened the way to adaptive and evolutive chemistry. Such highly sophisticated structures have also attracted broad interest in the surface chemistry community as solid surfaces provide versatile platforms for regulating and arraying metal–organic nanostructures.[4–6,10,11] Numerous on-surface investigations have demonstrated that coordination chemistry is an efficient strategy for forming various static metal–organic structures, such as well-defined surface-supported networks,[12–15] chains,[16–18] and clusters,[19–22] where usually only one kind of coordination binding site[12,13,15–17,19–22] or two different sites with similar coordination mode[14,18] are involved. Moreover, some studies have also shown that it is possible to induce structural transformations by regulation of metal/molecule stoichiometric ratios and/or temperature.[23–27] However, to our knowledge, these transformations were demonstrated to be nonreversible. Despite the well-known intrinsic reversibility of coordination bonds, systematic studies are still limited. More recently, such reversibility was shown in a simple system under ultrahigh vacuum (UHV) conditions where only two metal–organic coordination motifs with similar bonding mode are involved.[11] It is thus of general interest and a challenge to construct a more complicated system to achieve reversible structural transformations of multiple metal–organic motifs by virtue of different coordination binding modes, which gives access to constitutional diversity and adaptability. Such a model system should present particularly rich structural patterns on surfaces in response to the constituents, reversibly.

In this work, we chose a modified nucleobase, 9-ethylguanine (9eG; Scheme 1), as a potential candidate to interact with the transition metal Fe. The reason for choosing such a system is that: 1) the 9eG molecule contains two neighboring coordination binding sites (i.e., O6 and N7 sites, see Scheme 1, while the N3 site is potentially sterically hindered); 2) from the experimental findings[15] and also theoretical calculations, we conclude that the Fe atom preferentially coordinates with the O6 site.[19] It thus may allow us to construct a model system for investigating the coordination priority and diversity, and more importantly, to realize the reversible structural transformations on the surface under UHV conditions by virtue of intrinsic dynamic characteristics of coordination bonds. Herein, from the combination of high-resolution scanning tunneling microscopy (STM) and density functional theory (DFT) calculations, we show that: 1) by deposition of Fe atoms on a 9eG-precovered Au(111) surface at room temperature (RT) in a controlled stepwise dosage, we achieve the sequential formation of various surface nanostructures composed of metal–organic G_4Fe_1, heterochiral G_3Fe_1, G_4Fe_2, G_3Fe_3 and homochiral G_3Fe_1 motifs (Scheme 1) as elementary building blocks; 2) these processes are reversible by controlled deposition of additional 9eG on a certain structure-covered surface at RT; 3) such a system thus demonstrates reversible structural transformations on a solid

[a] C. Zhang,[+] L. Wang,[+] L. Xie, Y. Ding, Prof. Dr. W. Xu
Tongji-Aarhus Joint Research Center for Nanostructures and Functional Nanomaterials, College of Materials Science and Engineering
Tongji University, Caoan Road 4800, Shanghai 201804 (P.R. China)
E-mail: xuwei@tongji.edu.cn

[+] These authors contributed equally to this work.

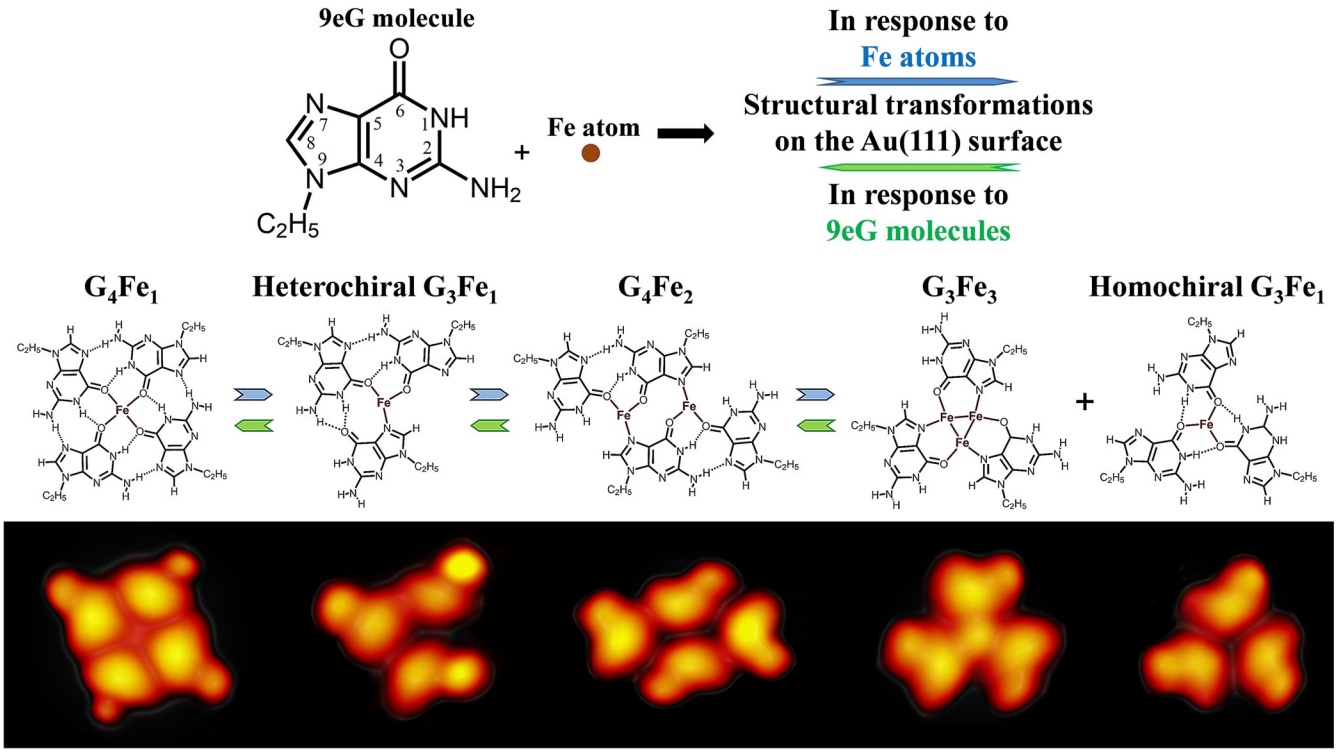

Scheme 1. Schematic illustration of the reversible structural transformations among G_4Fe_1, heterochiral G_3Fe_1, G_4Fe_2 and G_3Fe_3 together with homochiral G_3Fe_1 motifs in response to Fe atoms and 9eG molecules. The chemical structure of 9eG molecule is shown in the upper panel. The structural models and the corresponding high-resolution STM images of these metal–organic motifs are shown in the lower panel.

surface, in which controllable formation of multiple metal–organic motifs by use of different coordination binding modes can be dually responsive to metal atoms and molecules, is achieved under UHV conditions. The key to making these interconversions successful is the reversible characteristic of coordination bonds together with coordination priority and diversity. Furthermore, projected density of states (PDOS) and spin density analyses qualitatively demonstrate that the electronic and magnetic properties of Fe centers within the formed metal–organic motifs can be varied. These results may provide fundamental insights into the intrinsic dynamic characteristic of coordination chemistry, and also the controllable fabrication of nanostructures.

Results and Discussion

As previously demonstrated, the simultaneous co-deposition of 9eG molecules and Fe atoms on Au(111) held at RT results in the formation of G-quartet-Fe (i.e., G_4Fe_1) networks.[19] In this work, we try to explore the feasibility of structural transformations based on a sequential deposition method. To do so, we first deposited 9eG on the surface held at RT and obtained the self-assembled 9eG islands (Figure 1 a).[19] Before deposition of Fe atoms, delicate calibrations of Fe dosages were performed. We first tried to deposit Fe atoms on the bare surface to regulate the emission currents of the evaporator and durations. Then we tried to keep the molecular coverage ($\approx$0.5 monolayer) as a constant and varied the Fe dosages step-by-step (leading to a gradual transformation from 9eG islands to G-quartet-Fe (i.e., G_4Fe_1) networks as shown in Figure S1). Finally, we found that by using the emission current of $\approx$1.5 mA and duration of $\approx$5 min, most 9eG molecules ($\approx$0.5 monolayer) are in the form G_4Fe_1. We then took the above parameters as a reference. After calibrations, we then controllably deposited Fe on such a 9eG-precovered surface at RT and interestingly, obtained the G_4Fe_1 networks[19] (Figure 1 b). From such a sequential deposition method, we found that Fe atoms initially disturb the hydrogen-bonded 9eG islands from the edges, and then gradually interact with 9eG via preferential coordination to O6 sites (Scheme 1) to form the specific G_4Fe_1 motifs (Figure S1 in the Supporting Information).

As there are two neighboring binding sites (O6 and N7) within 9eG with the potential for coordination to Fe (i.e., coordination diversity),[14,18] based on the above findings and the intrinsic reversibility of noncovalent interactions, we systematically carried out further experiments and achieved a series of structural transformations (Figure 1 c–h). After further deposition of Fe on the G_4Fe_1-precovered surface at RT in a step-by-step manner, we gained an overview of the gradual structural transformations of various surface nanostructures involving diverse metal–organic motifs, namely, heterochiral G_3Fe_1 motifs (Figure 1 c, d), G_4Fe_2 (Figure 1 e, f), G_3Fe_3 and homochiral G_3Fe_1 (Figure 1 g, h). Note that all these structural motifs were ascribed by the specific metal/organic ratios as exhibited by the structural models in the middle row of Scheme 1. The corresponding zoom-in STM images and DFT calculated models (involving the compositions of these structures) will be discussed in detail in the following.

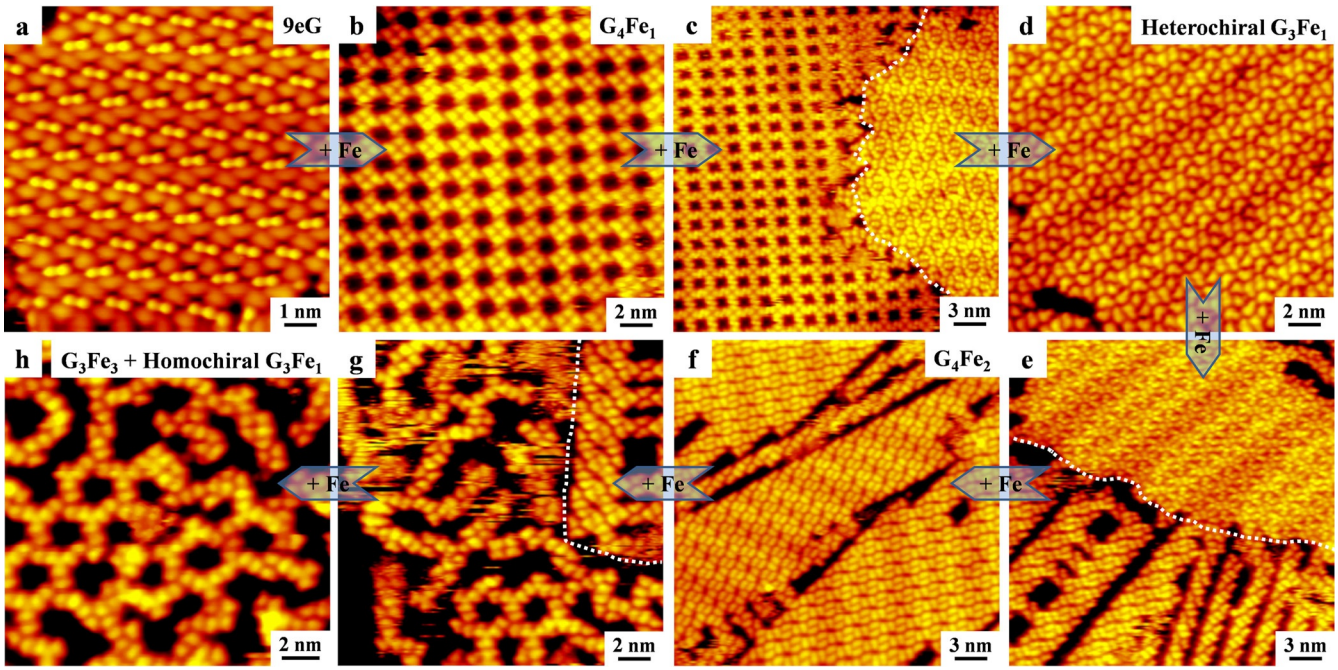

Figure 1. STM images showing the structural transformations in response to Fe atoms. a) Formation of the 9eG island at RT. Structural transformations among: b) G_4Fe_1, d) heterochiral G_3Fe_1, f) G_4Fe_2, and h) G_3Fe_3 together with homochiral G_3Fe_1 motifs on the Au(111) surface after stepwise dosing of Fe atoms on the sample obtained in the last step at RT. c,e,g) Coexistence of the two respective structures within the transformations. The white contours in the images indicate the structural boundaries, respectively. Scanning conditions: $I_t = 0.90$ nA, $V_t = 1200$ mV.

Interestingly, such structural transformations can be reversed stepwise through controlled depositions of 9eG on a certain structure-covered surface at RT (Figure 2). Such a system thus achieves continuous interconversions among multiple metal–organic motifs through reversible breakage and reformation of coordination bonds in response to both metal atoms and molecules. Note that all these coordination structures can also be formed by simultaneous co-deposition of 9eG and Fe at controlled ratios.

On the close-up STM image of Figure 1 d (Figure 3 a), the molecular island can be depicted by ribbons (separated by the white dotted lines) that are composed of trimers with opposite chiralities between neighboring ribbons as indicated by the black and blue contours. After extensive structural search, this elementary trimer was assigned to a heterochiral G_3Fe_1 metal–organic motif as superimposed on the STM image (Figure 3 b). From the DFT-optimized model, we found that this structure is formed by three 9eG molecules (with different chiralities) coordinating with one Fe atom by two O6 sites and one N7 site (also see Figure 3 c), and the intermolecular NH···O and NH···N hydrogen bonds further stabilize the motif. Then each G_3Fe_1 motif binds to the neighboring ones through double NH···N hydrogen bonds within the ribbons and single NH···N hydrogen bonds together with additional van der Waals forces (resulting from the ethyl groups) in between the ribbons as detailed in Figure S2.

From the close-up STM image of Figure 1 f (Figure 4 a), we found that the molecular island is composed of tetramers as separated by the white dotted lines. This elementary tetramer is assigned to a G_4Fe_2 metal–organic motif as highlighted in

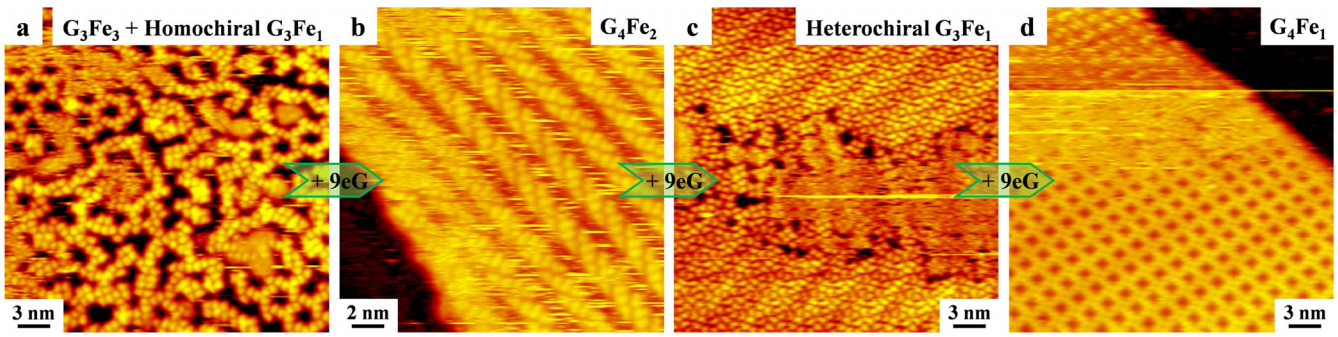

Figure 2. STM images showing the structural transformations from: a) G_3Fe_3 and homochiral G_3Fe_1, through b) G_4Fe_2, and then c) heterochiral G_3Fe_1 to d) G_4Fe_1 by step-by-step deposition of 9eG at RT.

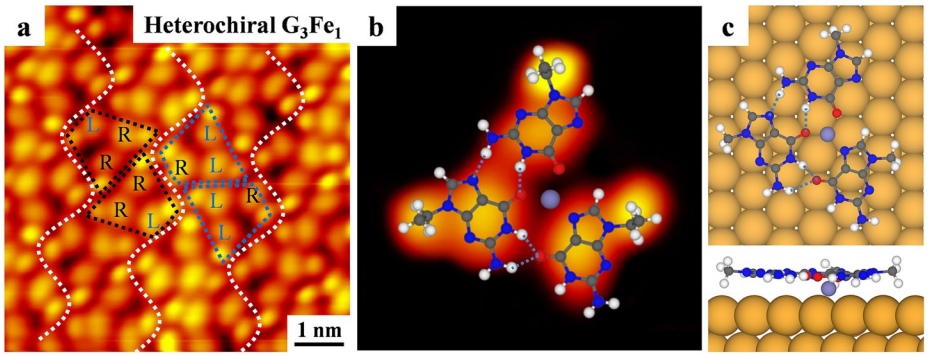

Figure 3. a) Formation of the island structure composed of the heterochiral G_3Fe_1 motifs after deposition of Fe atoms on the G_4Fe_1-precovered Au(111) surface held at RT. The submolecularly resolved STM image allows us to identify the molecular chiralities (as indicated by L and R notations). The elementary heterochiral G_3Fe_1 motifs are depicted by black and blue contours within each ribbon. Scanning conditions: $I_t = 0.90$ nA, $V_t = 1200$ mV. b) The close-up STM image of the heterochiral G_3Fe_1 motif superimposed with the DFT-optimized gas-phase structural model. c) Top and side views of the structural model of the heterochiral G_3Fe_1 motif (the ethyl group is replaced by a methyl group for simplicity) on Au(111); the hydrogen bonds are depicted by dashed lines. H: white; C: gray; N: blue; O: red. Fe: light purple.

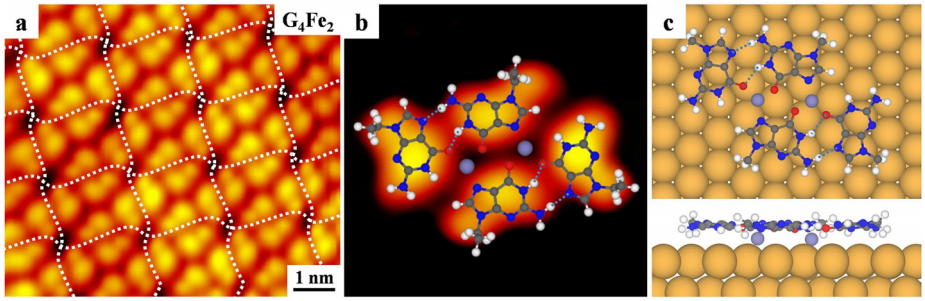

Figure 4. a) Formation of the island structure composed of the G_4Fe_2 motifs after deposition of Fe atoms on the heterochiral-G_3Fe_1-precovered Au(111) surface held at RT. The elementary G_4Fe_2 motifs are separated by white dotted lines for clarity. The submolecularly resolved STM image shows that the G_4Fe_2 motif is composed of homochiral 9eG molecules. Scanning conditions: $I_t = 0.90$ nA, $V_t = 1200$ mV. b) The close-up STM image of the G_4Fe_2 motif superimposed with the DFT-optimized gas-phase structural model. c) Top and side views of the structural model of the G_4Fe_2 motif on Au(111), where the hydrogen bonds are depicted by dashed lines.

Figure 4b. From the DFT-optimized model superimposed on the STM image, we found that it is formed by four 9eG molecules (with the same chirality) coordinating with two Fe atoms by two O6 sites and one N7 site for each, and the intermolecular NH···O and NH···N hydrogen bonds further stabilize the motif (also see Figure 4c). Then each G_4Fe_2 motif binds to the neighboring ones through double NH···N hydrogen bonds (Figure S3).

It is worth noting that after a closer inspection of the G_4Fe_1, heterochiral G_3Fe_1, and G_4Fe_2 motifs (Figure S4 in the Supporting Information), we identified that the structural formation and evolution exhibit the following intriguing aspects: 1) the preferential coordination between Fe atom and O6 site results in the formation of the specific G_4Fe_1 motif; 2) the N7 site becomes involved at higher Fe/9eG ratios (forming the heterochiral G_3Fe_1 motif and also G_4Fe_2) thus presenting coordination diversity; 3) in the structural-evolution process among these three motifs, we distinguished that G_4Fe_1 is only partially disturbed, as indicated by the white rectangles in Figure S4 where the traces of a half G-quartet motif still remain (with similar hydrogen-bonded configurations).

Further controlled deposition of Fe atoms at an even higher Fe/9eG ratio (e.g., $\approx$1:1) on the G_4Fe_2-precovered surface at RT resulted in the formation of hexagonal rings instead of island structures. From the STM image (Figure 5a), we found that the molecular rings are composed of trimers as depicted by the hexagonal contours, and could be assigned to G_3Fe_3 motifs (Figure 5b), where the tri-iron cluster (Fe_3) is resolved as a bright spot. Similar tri-metal clusters in metal–organic motifs were also reported previously.[21,22] From the superimposed DFT-optimized model, we found that this structures is formed by three homochiral 9eG molecules coordinating with three Fe atoms by occupying all of the available O6 and N7 sites simultaneously, and there are no potential intermolecular hydrogen bonds within the motif (also see Figure 5c). Then each G_3Fe_3 motif binds to the neighboring ones through double NH···N hydrogen bonds (Figure S5). Besides the G_3Fe_3 motif another kind of ring structure composed of slightly different trimers, as depicted by the triangular contours, was also observed to coexist on the surface (Figure 5d). This elementary trimer is assigned to a homochiral G_3Fe_1 motif (Figure 5e). In comparison with the G_3Fe_3 motif, the central bright spot disappeared in the homochiral G_3Fe_1. From the superimposed DFT-optimized model, we found that this structure is also formed by three homochiral 9eG molecules which coordinate with one Fe atom via three O6 sites only, and the intermolecular NH···O hydrogen

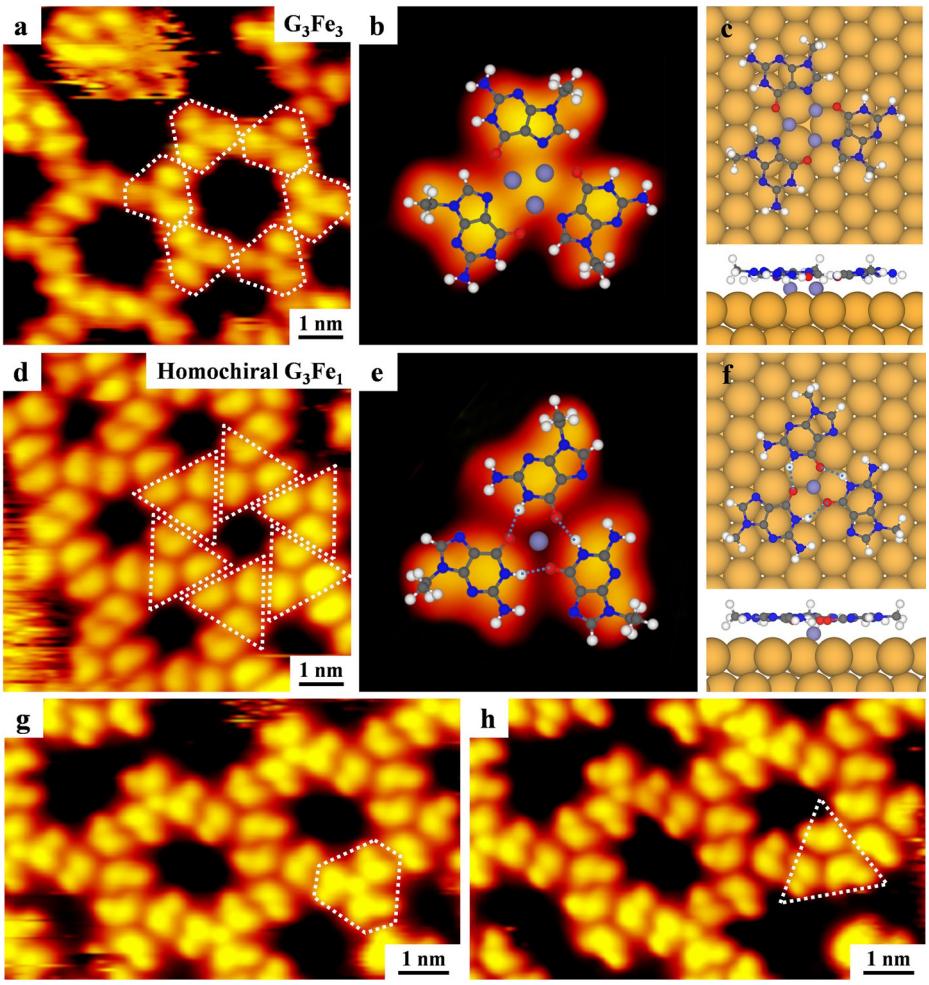

Figure 5. a, d) Formation of hexagonal rings composed of the G_3Fe_3 and homochiral G_3Fe_1 motifs after deposition of Fe atoms on the G_4Fe_2-precovered Au(111) surface held at RT. The elementary G_3Fe_3 and homochiral G_3Fe_1 motifs are depicted by white contours. The submolecularly resolved STM images show that both motifs are composed of homochiral 9eG molecules. Scanning conditions: $I_t = 0.90$ nA, $V_t = 1200$ mV. b, e) The close-up STM images of the G_3Fe_3 and homochiral G_3Fe_1 motifs superimposed with the DFT-optimized gas-phase structural models, respectively. c, f) Top and side views of the structural models of the G_3Fe_3 and homochiral G_3Fe_1 motifs on Au(111), respectively. g, h) Continuous STM images showing the structural transformation from the G_3Fe_3 motif to the homochiral G_3Fe_1 by lateral STM manipulations as highlighted by white contours.

bonds further stabilize the motif (also see Figure 5 f). Then each homochiral G_3Fe_1 motif also binds to the neighboring ones through double NH···N hydrogen bonds as detailed in Figure S5. Note that the structural assignments of G_3Fe_3 and homochiral G_3Fe_1 motifs are not only consistent with the molecular alignments determined from the high-resolution STM topography (e.g., the characteristic triangular part of guanine moiety and the position of ethyl group), but can also be rationalized by the intra- and intermotif hydrogen bonds. As mentioned above, in the structural-evolution processes among the G_4Fe_1, heterochiral G_3Fe_1, and G_4Fe_2 motifs, half of the G-quartets remain unperturbed (Figure S4). At a Fe/9eG ratio of ≈1:3, the heterochiral G_3Fe_1 motif is energetically more favorable than the homochiral G_3Fe_1 one as determined from DFT calculations.

It is interesting to note that at such a high Fe/9eG ratio (≈1:1) we naturally expected to obtain G_3Fe_3 motifs, but actually these motifs only accounted for ≈70% of the structures. Also, we tried to deposit more Fe atoms on the surface, and the additional Fe atoms were found to accumulate and form Fe clusters. Thus, it seems unreasonable to obtain the homochiral G_3Fe_1. By employing the same means as the one we employed with the G-quartet-Fe motif,[19] we were able to perturb G_3Fe_3 with the STM tip, which resulted in a structural transformation from G_3Fe_3 to the homochiral G_3Fe_1 (indicated by the different contours, where each molecule rotates a little bit with the release of Fe atoms) as shown in Figure 5 g and h. This process further demonstrates the dynamic characteristic of coordination bonds, and may well account for the appearance of homochiral G_3Fe_1 motifs that coexist with G_3Fe_3 (Figure 5 g). Such a process is also similar to the dynamic phenomenon of a coordination motif where the metal center was found to be able to jump in and out.[20] Metal–organic structural transformation by STM manipulation has been reported,[28] but in that case the coordination mode did not change, which is different from what is shown here.

As the system demonstrates the reversible structural transformations on Au(111), it was interesting to further explore the

electronic and magnetic properties of the Fe centers within these motifs because such properties could be influenced by the local chemical environments.[19,29–31] We then calculated the corresponding PDOS on the d orbitals of the individual Fe centers within these motifs on Au(111) and plotted their spin-density distributions (Figure S6 in the Supporting Information). From the PDOS plots, a large splitting between the spin-up and spin-down states of the individual Fe atoms in each motif can be identified (Figure S6e), indicating that the Fe centers are all strongly magnetized. Moreover, the spin-density distributions (Figure S6a–d) show that the spin densities are prominently around the Fe centers and also partly on O6 sites and fewer on N7 sites, indicating the spin polarization of O6 and N7 atoms by coordination with Fe atoms. As a result, the individual Fe center has a magnetic moment calculated to be 3.50, 3.47, 3.15, and 3.51 μ_B for heterochiral G_3Fe_1, G_4Fe_2, G_3Fe_3, and homochiral G_3Fe_1 motifs, respectively, which can also be confirmed from the energy intervals between the spin-up and spin-down d_{total} orbitals. The magnetic moment of the Fe center in the G_4Fe_1 complex on Au(111) has been reported to be 3.63 μ_B.[19] The induced small magnetic moments of O6 and N7 atoms are detailed in Figure S7. It is worth noting that for the G_4Fe_2 structure, both ferromagnetic and antiferromagnetic coupling of two Fe atoms were calculated to be very close in energy and no preference could be determined, which is similar to the cases reported previously.[32,33] The detailed spin-density distributions and PDOS plots are shown in Figure S8 in the Supporting Information. Therefore, we provide a strategy to control the electronic and magnetic properties of Fe-centered motifs by virtue of structural transformations.

Conclusions

In conclusion, we have systematically demonstrated the on-surface reversible structural transformations of multiple metal–organic motifs with different binding modes in response to both Fe and 9eG, where the intrinsic dynamic characteristic of coordination bonds and the coordination priority and diversity are found to be key. The strategy for fabrication of surface nanostructures with variation and selection by virtue of dynamic coordination chemistry may be extended to other more general cases.

Experimental Section

All STM experiments were performed in a UHV chamber (base pressure 1×10^{-10} mbar) equipped with a variable-temperature, fast-scanning "Aarhus-type" STM using electrochemically etched W tips purchased from SPECS,[34,35] a molecular evaporator and an e-beam evaporator, and other standard instrumentations for sample preparations. The Au(111) substrate was prepared by several cycles of 1.5 keV Ar^+ sputtering followed by annealing to 800 K for 15 min; this resulted in clean and flat terraces separated by monatomic steps. The 9eG molecules (purchased from Sigma–Aldrich, purity $>98\%$) were loaded into a glass crucible in the molecular evaporator. After a thorough degassing, the molecules were deposited onto the Au(111) substrate by thermal sublimation and then the Fe atoms were deposited onto the 9eG-precovered surfaces at RT, and the sample was thereafter transferred within the UHV chamber to the STM, where measurements were carried out at $\approx$100–150 K.

The calculations were performed in the framework of DFT by using the Vienna ab initio simulation package (VASP).[36,37] The projector-augmented wave method was used to describe the interaction between ions and electrons;[38,39] the Perdew–Burke–Ernzerhof generalized gradient approximation (GGA) exchange–correlation functional was employed,[40] and van der Waals interactions were included by using the dispersion-corrected DFT-D2 method of Grimme[41] for the calculations when including the gold surface. The atomic structures were relaxed by using the conjugate gradient algorithm scheme as implemented in the VASP code until the forces on all unconstrained atoms were $\leq$0.03 eV Å^{-1}.

Acknowledgements

The authors acknowledge the financial support from the National Natural Science Foundation of China (21473123, 21622307), the Research Fund for the Doctoral Program of Higher Education of China (20120072110045).

Keywords: coordination chemistry · density functional calculations · metal–organic frameworks · scanning tunneling microscopy · structural transformation

[1] B. J. Holliday, C. A. Mirkin, *Angew. Chem. Int. Ed.* **2001**, *40*, 2022–2043; *Angew. Chem.* **2001**, *113*, 2076–2097.
[2] B. H. Ye, M. L. Tong, X. M. Chen, *Coord. Chem. Rev.* **2005**, *249*, 545–565.
[3] M. Eddaoudi, D. B. Moler, H. Li, B. Chen, T. M. Reineke, M. O'keeffe, O. M. Yaghi, *Acc. Chem. Res.* **2001**, *34*, 319–330.
[4] J. V. Barth, *Surf. Sci.* **2009**, *603*, 1533–1541.
[5] N. Lin, S. Stepanow, M. Ruben, J. V. Barth, in *Templates in Chemistry III, Vol. 287*, Springer, Heidelberg, **2008**, pp. 1–44.
[6] S. Stepanow, N. Lin, J. V. Barth, *J. Phys. Condens. Matter* **2008**, *20*, 184002.
[7] J. M. Lehn, *Chem. Soc. Rev.* **2007**, *36*, 151–160.
[8] J. M. Lehn, *Angew. Chem. Int. Ed.* **2013**, *52*, 2836–2850; *Angew. Chem.* **2013**, *125*, 2906–2921.
[9] J. M. Lehn, *Proc. Natl. Acad. Sci. USA* **2002**, *99*, 4763–4768.
[10] A. Ciesielski, S. Lena, S. Masiero, G. P. Spada, P. Samorì, *Angew. Chem. Int. Ed.* **2010**, *49*, 1963–1966; *Angew. Chem.* **2010**, *122*, 2007–2010.
[11] H. Kong, C. Zhang, L. Xie, L. Wang, W. Xu, *Angew. Chem. Int. Ed.* **2016**, *55*, 7157–7160; *Angew. Chem.* **2016**, *128*, 7273–7276.
[12] H. Kong, Q. Sun, L. Wang, Q. Tan, C. Zhang, K. Sheng, W. Xu, *ACS Nano* **2014**, *8*, 1804–1808.
[13] F. Bebensee, K. Svane, C. Bombis, F. Masini, S. Klyatskaya, F. Besenbacher, M. Ruben, B. Hammer, T. R. Linderoth, *Angew. Chem. Int. Ed.* **2014**, *53*, 12955–12959; *Angew. Chem.* **2014**, *126*, 13169–13173.
[14] Q. Sun, L. Cai, H. Ma, C. Yuan, W. Xu, *Chem. Commun.* **2015**, *51*, 14164–14166.
[15] A. Langner, S. L. Tait, N. Lin, R. Chandrasekar, V. Meded, K. Fink, M. Ruben, K. Kern, *Angew. Chem. Int. Ed.* **2012**, *51*, 4327–4331; *Angew. Chem.* **2012**, *124*, 4403–4407.
[16] T. Classen, G. Fratesi, G. Costantini, S. Fabris, F. L. Stadler, C. Kim, S. de Gironcoli, S. Baroni, K. Kern, *Angew. Chem. Int. Ed.* **2005**, *44*, 6142–6145; *Angew. Chem.* **2005**, *117*, 6298–6301.
[17] D. Skomski, C. D. Tempas, K. A. Smith, S. L. Tait, *J. Am. Chem. Soc.* **2014**, *136*, 9862–9865.
[18] D. Skomski, C. D. Tempas, G. S. Bukowski, K. A. Smith, S. L. Tait, *J. Chem. Phys.* **2015**, *142*, 101913.
[19] L. Wang, H. Kong, C. Zhang, Q. Sun, L. Cai, Q. Tan, F. Besenbacher, W. Xu, *ACS Nano* **2014**, *8*, 11799–11805.
[20] N. Lin, A. Dmitriev, J. Weckesser, J. V. Barth, K. Kern, *Angew. Chem. Int. Ed.* **2002**, *41*, 4779–4783; *Angew. Chem.* **2002**, *114*, 4973–4977.

[21] H. Kong, L. Wang, Q. Tan, C. Zhang, Q. Sun, W. Xu, *Chem. Commun.* **2014**, *50*, 3242 – 3244.
[22] H. Kong, L. Wang, Q. Sun, C. Zhang, Q. Tan, W. Xu, *Angew. Chem. Int. Ed.* **2015**, *54*, 6526 – 6530; *Angew. Chem.* **2015**, *127*, 6626 – 6630.
[23] A. Dmitriev, H. Spillmann, N. Lin, J. V. Barth, K. Kern, *Angew. Chem. Int. Ed.* **2003**, *42*, 2670 – 2673; *Angew. Chem.* **2003**, *115*, 2774 – 2777.
[24] J. Liu, T. Lin, Z. Shi, F. Xia, L. Dong, P. N. Liu, N. Lin, *J. Am. Chem. Soc.* **2011**, *133*, 18760 – 18766.
[25] D. Ecija, S. Vijayaraghavan, W. Auwärter, S. Joshi, K. Seufert, C. Aurisicchio, D. Bonifazi, J. V. Barth, *ACS Nano* **2012**, *6*, 4258 – 4265.
[26] M. Pivetta, G. E. Pacchioni, E. Fernandes, H. Brune, *J. Chem. Phys.* **2015**, *142*, 101928.
[27] T. C. Tseng, N. Abdurakhmanova, S. Stepanow, K. Kern, *J. Phys. Chem. C* **2011**, *115*, 10211 – 10217.
[28] D. Heim, K. Seufert, W. Auwärter, C. Aurisicchio, C. Fabbro, D. Bonifazi, J. V. Barth, *Nano Lett.* **2010**, *10*, 122 – 128.
[29] A. Zhao, Q. Li, L. Chen, H. Xiang, W. Wang, S. Pan, B. Wang, X. Xiao, J. Yang, J. G. Hou, Q. Zhu, *Science* **2005**, *309*, 1542 – 1544.
[30] V. Iancu, A. Deshpande, S. W. Hla, *Phys. Rev. Lett.* **2006**, *97*, 266603.
[31] L. Gao, W. Ji, Y. B. Hu, Z. H. Cheng, Z. T. Deng, Q. Liu, N. Jiang, X. Lin, W. Guo, S. X. Du, W. A. Hofer, X. C. Xie, H. J. Gao, *Phys. Rev. Lett.* **2007**, *99*, 106402.
[32] A. P. Seitsonen, M. Lingenfelder, H. Spillmann, A. Dmitriev, S. Stepanow, N. Lin, K. Kern, J. V. Barth, *J. Am. Chem. Soc.* **2006**, *128*, 5634 – 5635.
[33] H. Wende, M. Bernien, J. Luo, C. Sorg, N. Ponpandian, J. Kurde, J. Miguel, M. Piantek, X. Xu, Ph. Eckhold, W. Kuch, K. Baberschke, P. M. Panchmatia, B. Sanyal, P. M. Oppeneer, O. Eriksson, *Nat. Mater.* **2007**, *6*, 516 – 520.
[34] F. Besenbacher, *Rep. Prog. Phys.* **1996**, *59*, 1737 – 1802.
[35] E. Laegsgaard, L. Österlund, P. Thostrup, P. B. Rasmussen, I. Stensgaard, F. Besenbacher, *Rev. Sci. Instrum.* **2001**, *72*, 3537 – 3542.
[36] G. Kresse, J. Hafner, *Phys. Rev. B Condens. Matter Mater. Phys.* **1993**, *48*, 13115.
[37] G. Kresse, J. Furthmüller, *Phys. Rev. B Condens. Matter Mater. Phys.* **1996**, *54*, 11169.
[38] P. E. Blöchl, *Phys. Rev. B Condens. Matter Mater. Phys.* **1994**, *50*, 17953.
[39] G. Kresse, D. Joubert, *Phys. Rev. B Condens. Matter Mater. Phys.* **1999**, *59*, 1758.
[40] J. P. Perdew, K. Burke, M. Ernzerhof, *Phys. Rev. Lett.* **1996**, *77*, 3865.
[41] S. Grimme, *J. Comput. Chem.* **2006**, *27*, 1787 – 1799.

Manuscript received: October 16, 2016
Accepted Article published: December 19, 2016
Final Article published: January 18, 2017